Sustainable Cities and Society 109 (2024) 105547

Contents lists available at ScienceDirect

Sustainable Cities and Society

journal homepage: www.elsevier.com/locate/scs

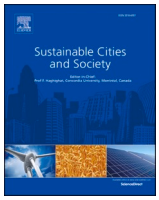

The application of a high-density street-level air temperature observation network (HiSAN): Spatial and temporal variations of thermal and wind condition in different climatic condition types

Yu-Cheng Chen [a,*], Kai-Shan Hou [b], Yu-Jie Liao [b], Tsuyoshi Honjo [c], Fang-Yi Cheng [d], Tzu-Ping Lin [b]

[a] Department of Architecture, Nanhua University, No. 55, Sec. 1, Nanhua Rd., Dalin Township, Chiayi County 62249, Taiwan
[b] Department of Architecture, National Cheng Kung University, 1 University Rd., East Dist., Tainan 701, Taiwan
[c] Graduate School of Horticulture, 648 Matsudo, Matsudo-shi, Chiba 271-8510, Japan
[d] Department of Atmospheric Sciences, National Central University, 300, Zhongda Rd., Zhongli District, Taoyuan 320, Taiwan

ARTICLE INFO

Keywords:
Urban Heat Island
Observations network
Wind condition
Thermal condition
Climatic condition types

ABSTRACT

Different patterns of urban development will result in different characteristics of the urban heat island effect (UHI). In order to explore the impacts of urban environment characteristics, wind conditions, and climatic condition types on UHI over different periods, this study adopted Tainan City as the study site, and utilized the surface roughness length and wind prediction, to evaluate the correlation between wind conditions and UHI, as well as the thermal environment affected by different environmental. The UHI characteristics were evaluated by using 100 measurement stations (HiSAN) located in different urban environments. The results revealed the expansion of the daily temperature range was associated with an increase in the eastwest UHI centroid point movement; wind conditions affected north-south shifts of UHI centroid point. The built environments was positively correlate with daytime (0.24) and nighttime (0.68) temperatures. Daytime water bodies notably cool surroundings (correlation -0.52), and green spaces enhance nighttime cooling (correlation -0.64). Wind speed negatively correlates with UHI deviation values during the daytime (-0.17) and nighttime (-0.58). The study highlights the impact of wind speeds and temperature ranges on UHI movement, emphasizing effective ventilation's role in urban cooling and quantifying the importance of water and green space in mitigating UHI.

1. Introduction

Owing to the rapid urbanization process, the increase in population density, and the proliferation of artificial surfaces, anthropogenic heat emission, and heat stored in buildings have exacerbated thermal stress in urban areas, resulting in higher temperatures compared to suburbs. This phenomenon is known as the Urban Heat Island effect (UHI) (Baker et al., 2002). Previous studies have also revealed that the urban development characteristics affects the intensity of the UHI (Sobstyl et al., 2018; Anjos et al., 2020; Sangiorgio et al., 2020).

In recent years, the topic of UHI has been widely discussed. Many studies have proposed various methods for observing UHI, including measurements, modeling, and remote sensing (Saaroni et al., 2000; Heusinkveld et al., 2010; Kaloustian and Bechtel, 2016; Lin et al., 2017; Liu et al., 2017; Chen et al., 2016; Son et al., 2017; Mikami et al., 2011; Chen et al., 2018). The measurement data can truly characterize the UHI in urban scale, and when a sufficient number of measurement points are uniformly distributed in different urban development environments, the causes and effects of UHI can be more easily comprehended (Honjo, 2019; An et al., 2020; Richard et al., 2021; Cecilia et al., 2023).

In addition to thermal conditions, studies have shown that wind conditions are another factor closely related to UHI (Rajagopalan et al., 2014; Müller et al., 2014; Zong et al., 2021; Al-Obaidi et al., 2021; Luo et al., 2023). The dense arrangement of tall buildings not only narrows urban spaces, obstructing the view of the sky, but also hinders ventilation in the city (Yuan and Ng, 2012). Artificial heat tends to stay in narrow streets, making dispersion difficult and leading to higher thermal conditions and poor air quality. Previous studies have shown that

Types of contributions: Full Length Article

* Corresponding author at: Department of Architecture, Nanhua University, No. 55, Sec. 1, Nanhua Rd., Dalin Township, Chiayi County 62249, Taiwan.
E-mail address: leo2208808@gmail.com (Y.-C. Chen).

https://doi.org/10.1016/j.scs.2024.105547
Received 29 January 2024; Received in revised form 13 April 2024; Accepted 20 May 2024
Available online 21 May 2024

effective urban ventilation will contribute to reducing the intensity of UHI (Shi et al., 2022; Kwok et al., 2022).

Control of the wind condition is also included in urban planning regulations in different regions. For example, the Hong Kong government has addressed the issue of urban natural ventilation by using the air ventilation assessment (AVA) to evaluate wind conditions and improve the living environment by calculating the proportion of the area occupied by a base area (Ng, 2004; Ng, 2009; Weerasuriya et al., 2008).

Similarly, Japan's Comprehensive Assessment System for Building Environment Efficiency (CASBEE) has established an assessment manual to discuss urban heat islands. It recommends various urban planning and design methods, such as windward areas of buildings, building shape, and layout, to achieve better urban cooling and ventilation benefits (Murakami et al., 2007; Japan Sustainable Building Consortium, 2014).

In Germany, the Federal Nature Protection Act (Gesetz über Naturschutz und Landschaftspflege, BnatSchG) explicitly mandates the assessment of building forms to preserve areas capable of generating fresh or cool air and to maintain adequate ventilation pathways.

In terms of thermal condition information, this study applied the high-density street-level air temperature observation network (HiSAN), comprising 100 measurement points, which has been widely used to detect UHI in Tainan for eight years since 2016 (Chen et al., 2018; Chen et al., 2019).

Various characteristics of UHI in Tainan have been found by correlating HiSAN information with geographic and built environment features. Results show that urban features have different effects on thermal conditions at different times. For example, green areas have a better cooling effect in the night, because of the continuous evapotranspiration of vegetation at night, and the artificial pavement on the surface of the green areas dilute the cooling capacity in daytime. The built-up areas near the coast offer better cooling effect in daytime due to the excellent heat absorption and storage capacity of water (Chen et al., 2019). HiSAN also helps identify UHI centroid points (UHICP), which dynamically move from west to east during the daytime and vice versa at night (Chen et al., 2018). Therefore, the Therefore, HiSAN is a reliable system for obtaining thermal condition information in Tainan city.

In terms of wind condition information, measuring wind conditions over a wide range is challenging, and air flow through urban areas is influenced by various factors such as surface undulation and fluid viscosity (Wong et al., 2010; Chen et al., 2017). Therefore, many of the studies in the past have utilized surface roughness lengths (SRL) to evaluate wind conditions over a defined range of scales (Chen et al., 2017; Hintz et al., 2020; Shen et al., 2022). Therefore, this study combines urban land cover data, digital elevation model (DEM), and digital surface model (DSM) to obtain information on altitude and obstacle areas, then estimates the SRL in the urban area. Pedestrian-level wind speed (WS) in different districts can be estimated by boundary WS and different land patterns.

Therefore, this study aims to combine the information on thermal, wind, and background climate conditions in urban areas to discuss the relationship between built environment. By understanding this interrelationship through quantitative data, it can provide planning references to improve future city climate quality considerations. The main issues of this study are as follows:

First, wind condition assessment, such as computational fluid dynamics (CFD) simulations, wind tunnel experiments, and field measurements, is difficult to obtain for a wide range of wind conditions in urban areas.

Second, previous studies have mainly explored the impact of urban environmental factors on UHI conditions; however, wind conditions also has high application potential for reducing the urban heat island.

Third, there are obvious differences between the wind condition and the thermal condition under various temporal and spatial backgrounds. Therefore, diversified analysis modes are required for different time periods to provide urban cooling strategies.

This study uses HiSAN to conduct long-term measurements of air temperature (Ta) under different meteorological conditions and uses the WS estimated by SRL characteristics to predict and analyze the measured data and related environmental factors to achieve the following purposes:

First, to use land surface features to provide a simple way to predict the wind condition at the pedestrian scale: In the past, a wide range of wind condition assessments often required considerable resources. Planning designers were less able to afford such long-term simulations and experiments in the primary design stage. Therefore, this study establishes a simple assessment method through surface features and predicts the wind condition at pedestrian scales in different regions.

Second, to analyze the relationship between wind and thermal conditions in Tainan City: Explore the microclimate conditions of Tainan with high spatial and temporal resolution. Understand which environmental and climatic factors dominate the Ta in different seasons and time periods in Tainan City and how to achieve a cooling effect through methods.

Third, to comprehend UHI and the distribution of ventilation potential under different climatic condition types (CCT): Past studies have found different temperature distributions at different time periods but rarely discussed them through wind conditions. This study will conduct large-scale research and analysis of climate patterns through the classification and screening of climate patterns, exploring the relationship between WS and Ta through the UHI characteristics including the UHICP movement, diurnal temperature range (DTR), and UHI deviation (UHID).

2. Method

2.1. Background information

2.1.1. Study area

The research area encompasses Tainan City (Fig. 1). According to data from the Tainan station under the Central Weather Bureau (CWB), the average Ta from 1981 to 2010 was 24.3 ℃. January and July were identified as the coldest and hottest months, respectively. The environmental wind field within the research area is observable throughout the year, with the prevailing wind direction primarily influenced by the northeast monsoon and northerly wind (Central Weather Bureau of Taiwan, 2021).

2.1.2. Research structure

In Fig. 2, the data collection of this study and the process of producing the results and the corresponding applications are shown. First, the basic data are divided into two categories: built environment and meteorological data. The built environment data mainly consists of the land cover data obtained from satellite imagery and the height information of surface objects obtained from light detection and ranging (LiDAR). The climate data is composed of the temperature data from HiSAN, the WS data obtained from CWB, and CCT based on prior research.

In the part of the research methodology that guides to the exploration of results, the proportion of land cover data is correlated with the Ta information from HiSAN during day and night, and the land cover with height information is used to calculate the SRL and combined with the WS data from the CWB to estimate the WS in different regions for understanding the effect of WS on the Ta. Additionally, the movement of the UHICP was analyzed horizontally and vertically, and correlated with climate patterns and thermal conditions.

Finally, this research is expected to apply the findings of the study to the development of sustainable city. Therefore, by suggesting land cover patterns and the reasons for the movement of the UHICP, it can be feedback to the recommendations of the urban planning, and the relationship between ventilation and cooling can be applied to the urban design review to propose regulations for the site configuration.

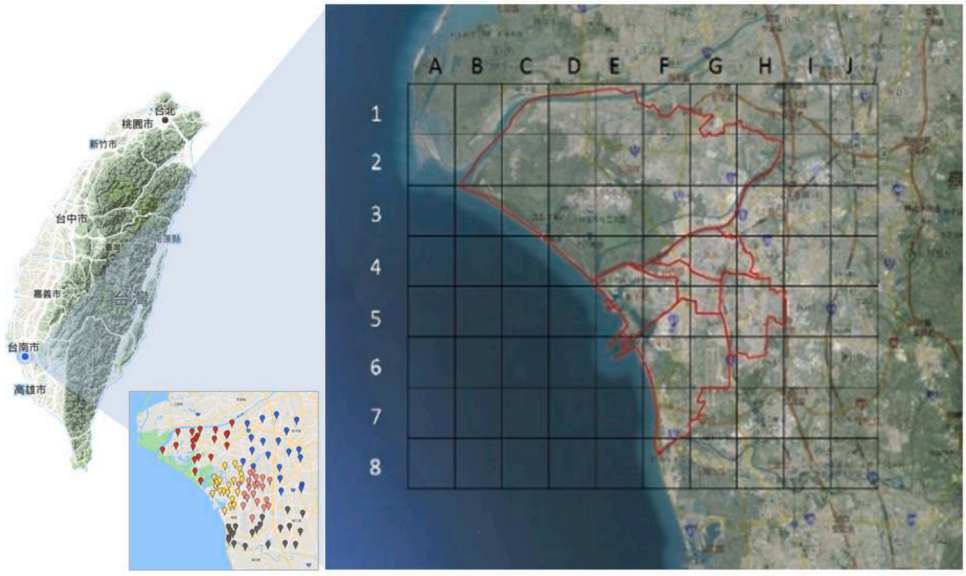

Fig. 1. Study area-Tainan City.

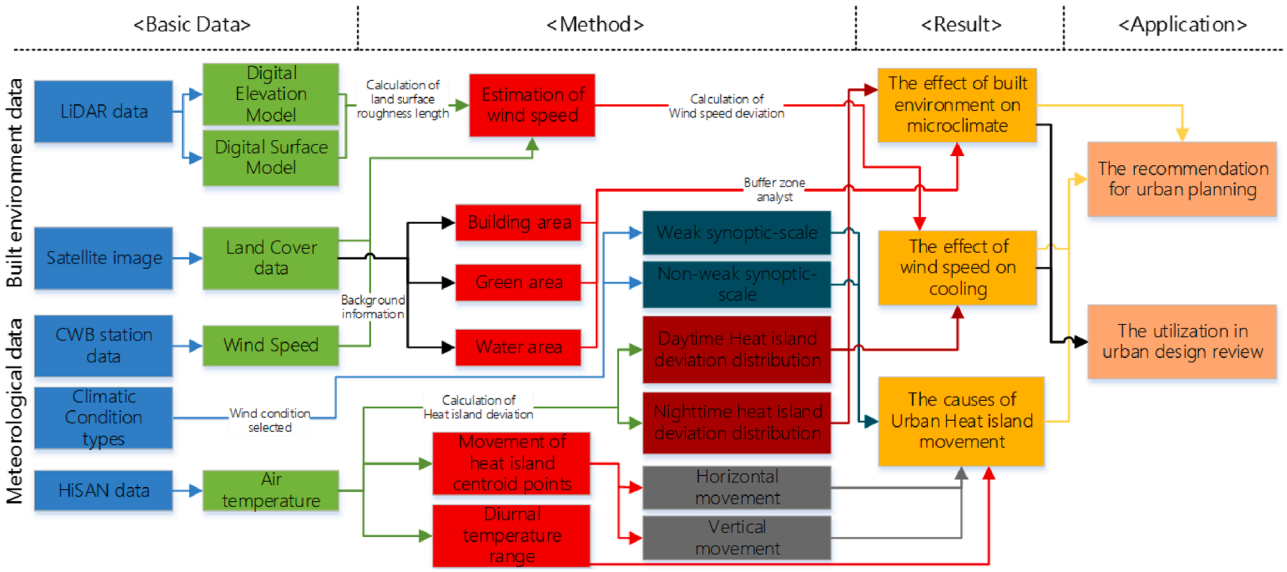

Fig. 2. Research structure.

2.2. *Measurement of thermal condition*

2.2.1. *HiSAN*

This study primarily utilizes HiSAN to acquire hourly temperature distribution within the study area (Fig. 3). Employing the principle of net mining homogenization, the entire Tainan research area is subdivided into grids with a side length of 2.75 kilometers. Each grid features at least one set of stations positioned at a height of 2.5 meters from the pedestrian level.

The Ta measuring instrument used is the Logpro model SD-185 temperature and humidity recorder, with a measurement interval of 100 seconds and an accuracy of ±0.5 ℃. To shield the instrument from direct sunlight and prevent water ingress, the temperature and humidity recorder is placed within a set of sensor weather shields and securely fixed to utility poles using U-shaped rings and hardware iron parts.

Data calibration and screening by HiSAN in this study proceed through the following steps:

First, before deploying the instrument outdoors for recording, it undergoes a two-day placement alongside two regularly calibrated instruments. On the day of instrument replacement, data is downloaded to confirm the accuracy of each instrument. If the temperature value deviates more than 0.5 ℃ from the instrument calibrated at the same time, it is not used for that day and sent back to the manufacturer for calibration.

Second, after instrument retrieval, the battery condition is checked to ensure it is in good condition. Subsequently, the temperature situation and the deviation of the average temperature for the day are assessed.

Previous studies employing HiSAN have identified numerous UHI features in Tainan and explored the influence of urban land-use differences on microclimate (Chen et al., 2018; Chen et al., 2019). Consequently, through the 100 densely distributed measurement points of HiSAN and the temperature data with high temporal resolution, this study not only obtains Ta information with high temporal and spatial accuracy, but also effectively identifies the distribution of UHI in Tainan City in different time. In addition, benefiting from the high resolution

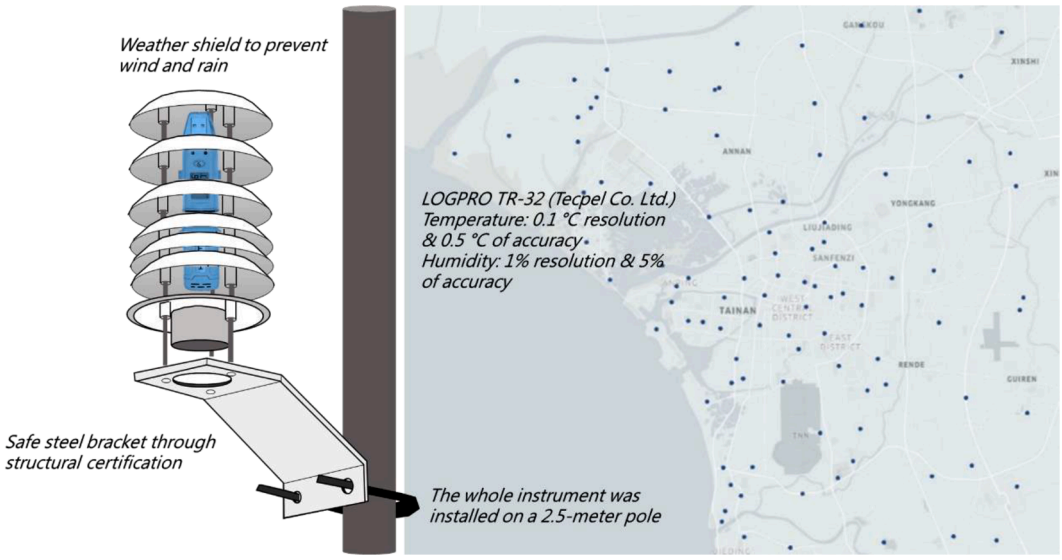

Fig. 3. HiSAN and the distribution in Tainan City.

advantage of HiSAN in UHI spatial and temporal variations, this study can effectively analyze the impacts of different land cover features on Ta in different periods, which will help urban planners and policy makers to develop mitigation strategies for high heat risk areas.

2.2.2. Air temperature data

Since this study primarily addresses the overall Ta distribution in the entire Tainan area, it is essential to interpolate the hourly temperature data from HiSAN between measurement points to gain insights into UHI conditions and understand differentiated Ta profiles based on land cover types.

This study uses MATLAB and the following commands and steps are employed for temperature interpolation between measuring points. Initially, the hourly Ta data and latitude and longitude coordinates of each measuring point are organized, utilizing the mesh grid function. The mesh grid command transforms the latitude and longitude coordinates of the entire research range into a continuous matrix, providing the basic data required for subsequent commands such as mesh and surf commands.

For the scattered data with coordinate positions and Ta data in this study, the grid data command, a 2-D and 3-D interpolation command, is used to calculate the Ta between measurement points. It's important to note that the grid data command only interpolates the scattered data points; it does not extrapolate the data. Therefore, the data generated defines only the smallest convex polygon formed by these data points, rather than forming a rectangular area of information.

During grid data interpolation, having more scattered data points is beneficial, and the data distribution should be averaged to better align with the correct peak distribution.

2.2.3. Urban heat isalnd deviation calculation

In this study, UHID is employed as a crucial indicator to assess the thermal condition at each site. It is calculated by taking the difference between the average Ta of each site and the average Ta of all sites, as shown in Eq. 1. UHID will be utilized in this study to evaluate its correlation with the ratio of the area covered by various environmental factors at each measurement point, including buildings, green areas, water, etc. The aim is to explore the influence of these environmental factors on the UHID at different time periods.

$$\mathrm{UHID} = \mathrm{t_i} - \frac{1}{\mathrm{n}}\sum_{\mathrm{i=1}}^{\mathrm{n}} \mathrm{t_i} \quad \text{(Eq 1)}$$

2.2.4. Quantify urban heat island movement characteristics

In this study, the analysis and discussion focus on UHICP and Ta distribution. The location of the UHICP can effectively represent the relatively hot part of the entire research area. The calculation of the UHICP is initially conducted at 100 points during this period. Subsequently, the temperature value t_i of each measuring point in this period to subtracted from t_{ave} to obtain the UHID value h_i of this measuring point in this period, as shown in Eq. 2.

$$t_{ave} = \frac{1}{n}\sum_{i=1}^{n} t_i \quad \text{(Eq 2)}$$

Subsequently, Eq. 3 is applied to multiply and sum the coordinates using the UHID values of each station and their absolute longitude and latitude. The result is then divided by the total of the UHID values of each station during the period to obtain the coordinates location of UHI centroid point (Loc_c). When calculating Loc_c, the position of coordinates both latitude and longitude directions needs to be carried out separately.

$$Loc_c = \frac{\sum_i^n l_i \times h_i}{\sum_i^n h_i} \quad \text{(Eq 3)}$$

$$(h_i = h_i \ if \ h_i \geq 0, \ h_i = 0 \ if \ h_i < 0)$$

To further examine the variations in the paths of UHICP, this study defines the length of UHICP movement for different dates as the maximum longitude value minus the minimum value of UHI centroid point on that day (L_x) as shown in Eq. 4. This study uses the L_x parameter to establish correlations with various climatic characteristics. For instance, it explores whether differences in WS and the DTR are the factors influencing the differential paths of UHICP, as depicted in Fig. 4.

$$L_x = L_{x\_max} - L_{x\_min} \quad \text{(Eq 4)}$$

L_{x_max}:The maximum longitude of the UHI centroid point on that day
L_{x_min}:The minimum longitude of the UHI centroid point on that day

2.3. Evaluation of wind condition

In this study, WS data from both standard and automatic stations established by the CWB are utilized, along with the built environment map of Tainan, which includes information on height and coordinates.

Assuming that the wind speed above the boundary layer is not influenced by surface undulation, the WS data from the standard meteorological stations in Tainan are adjusted by calculating the SRL of

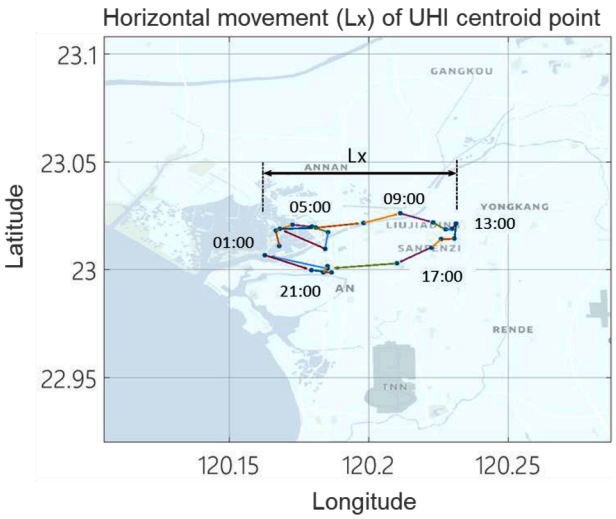

Fig. 4. Schematic of the longitudinal distance of UHI centroid point movement.

each grid. This adjustment allows for obtaining the distribution of hourly wind speed throughout the entire study area, as detailed in Section 2.3.4 below.

2.3.1. Land cover classification

In this study, Spot6 satellite images were employed for land cover identification using a supervised classification approach. The land cover was divided into five categories: buildings, water, soil, greenery, and roads, with an accuracy of 93 % (Fig. 5).

Through the classification of land cover, valuable information such as the area occupied by each category of land in different regions is obtained. This information is then used to calculate the SRL and estimate WS based on the proportion ratio of each land cover type. This approach allows for a comprehensive understanding of the relationship between different built environments and wind conditions.

2.3.2. Height information from LiDAR data

Given that this research focuses on the impact of wind condition caused by different terrain conditions, LiDAR is recognized as the most accurate method for detecting the height of ground objects. LiDAR, utilizing laser-ranging technology with precise direct geographic positioning in the air, can accurately establish DSM and DEM, allowing for detailed inspection and quantification of topographic features. Consequently, LiDAR technology has been increasingly employed in recent years to scan large areas and obtain three-dimensional information about the land.

In this study, the DSM and DEM data obtained from LiDAR were subtracted to derive the height of ground objects. Subsequently, this objects height data were overlaid with the surface coverage classification to obtain corresponding height values for each coverage area. These height values serve as a crucial factor in estimating SRL in this study.

2.3.3. Calculation of the land roughness length

SRL is a crucial indicator for quantifying land surface conditions, representing the level of surface undulation within a given area. Simultaneously, variations in SRL lead to different WS profiles that decrease with height (Oke, 1982; Oke et al., 2017).

In this study, the range used to calculate SRL is defined as 50 meters in a grid and using land cover and objects height data, enabling the extraction of three-dimensional features of the land.

In the SRL calculation, the emphasis is on the proportion of different surface coverages within the grid and the average height of each land surface block. The calculation approach in this research follows the equation (Kondo and Yamazawa, 1986), categorized as shown in Eq. 5.

$$Z_0 = (0.25 \cdot A_{build} \times H_{build}) + (0.125 \cdot A_{veg} \times H_{veg}) + (0.01 \cdot A_{open} \times 0.1m) \quad \text{(Eq 5)}$$

A_{build}: Building coverage proportion in a grid
A_{veg}: Vegetation coverage proportion in a grid
A_{open}:Open area coverage proportion including soil and road in a grid
(H_{build}):Average height of building
(H_{veg}):Average height of vegetation

2.3.4. Estimation of wind speed

Due to the vast size of the study area and the limited number of weather stations with WS information in the region, an overall understanding of the wind condition in the study area was obtained by using the calculation of the SRL of the grids.

In this study, the following steps were employed to estimate WS and illustrate the distribution of wind conditions across the entire study area:

Firstly, the SRL of each grid is calculated using the formula and then converted into the ground condition coefficient (α) (Bagiorgas et al., 2008; Oyedepo et al., 2012; Rasham, 2016). This α represents the WS profile and is determined through Eq. 6.

Fig. 5. Land cover classification in Tainan City.

$$\alpha = 0.096\log_{10}Z_0 + 0.0166\left(\log_{10}Z_0\right)^2 + 0.24 \quad \text{(Eq 6)}$$

Secondly, after obtaining the hourly WS and the height information of the CWB station, the WS measured by the CWB station can be converted to the WS at the average boundary layer height using the power law model for wind profiles (Counihan, 1975) within the study area, as shown in Eq. 7.

$$\overline{u}_{Z1} = \overline{u}_{Z2}\left[\frac{z_1}{z_2}\right]^{\alpha} \quad \text{(Eq 7)}$$

$\overline{u}_{Z1}$:*Wind speed in* Z_1 *(m/s)*
$\overline{u}_{Z2}$:*Wind speed in* Z_2 *(m/s)*
Z_1:*Height of* Z_1 *(m)*
Z_2:*Height of* Z_2*(m)*

Thirdly, this study assumes that the WS in the boundary layer height which set to 500 m in the Tainan area remains constant. The WS at the 500 m boundary layer can then be reduced to the WS at the pedestrian layer height of 2 m by Eq. 7. Therefore, this grid-based WS calculation process is employed to obtain distribution information for the entire study area (Fig. 6).

2.4. Climatic condition types

2.4.1. Classification of climatic condition types

The data sources utilized in this study include sixteen weather stations operated by the CWB of Taiwan, covering the period from January 2013 to March 2018, spanning a total of 1881 days. The classification of CCT for each date was based on prior research (Cheng and Hsu, 2019), which employed a two-stage cluster analysis method utilizing WS, wind direction, and pressure field data.

The CCT in this study are classify into six clusters:

1. Northeast monsoon: Characterized by the prevailing strong northeast monsoon winds, with the highest average WS among all cluster types.
2. Outflow rebound of the High Pressure: Northeast winds primarily affect northern Taiwan, with relatively poor diffusion conditions in the central and southern areas.
3. Weak synoptic scale: Taiwan is generally not influenced by any prominent synoptic system, resulting in low local impact from the wider environmental system and overall weak wind speeds.
4. Seasonal shift northeast monsoon: Affected by the weak seasonal shift northeast monsoon, occurring during the spring and fall seasonal shift months..
5. Subtropical high: Prevailing winds in Taiwan come from the south and southeast, leading to high Ta and more precipitation, resulting in fewer pollution events.
6. Summer weak synoptic: The influence of subtropical high pressure gradually decreases, with prevailing southwest and south winds and weaker WS in Taiwan.

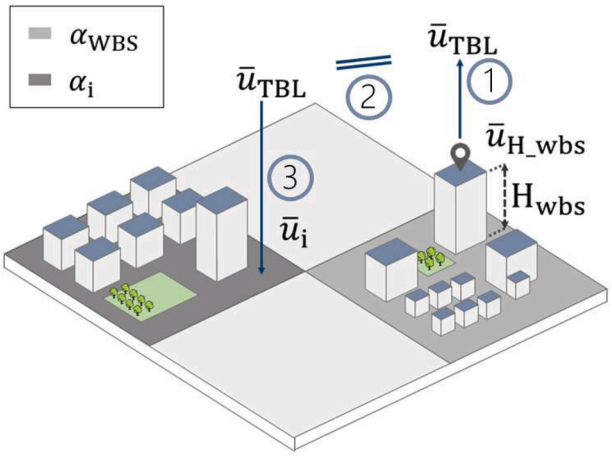

Fig. 6. Illustration of wind speed conversion process
$\overline{u}_{CWB}$:*wind speed in CWB station*
$\overline{u}_{ABL}$:*wind speed in atmospheric boundary layer*
$\overline{u}_i$:*wind speed 2m height in target region*
α_{CWB}:*ground condition coefficient in the grid that CWB station located*
α_i:*ground condition coefficient in target region.*

2.4.2. Screening of climatic conditions types

In this study, CCT were analyzed using the aforementioned classification method to conduct a comparative analysis of different climate backgrounds. The results of the climate grouping demonstrate that each month has its unique composition (Fig. 7).

From Fig. 7, it is evident that there are variations in the climate composition for each month, with slight differences between the CCT represented in winter and summer. This study delves into the thermal and wind conditions for different climate subgroups, aiming to investigate whether there are differences in Ta distribution across various climate backgrounds during the same period. For instance, varying WS and even distinct climate types may lead to different trends in the distribution of high-temperature masses in the same month.

2.4.3. Climatic condition types and wind and thermal condition

In this study, the Ta and WS information were analyzed based on the grouping of different CCT. The distribution of the thermal condition in the Tainan region was described by calculating UHICP and combining them with spatial information to illustrate the relationship between Ta and spatial and temporal changes in the Tainan region.

To effectively investigate the reasons for differences in the two-dimensional spatial presentation of UHICP, the movement was divided into longitude and latitude to understand individual causes.

In this study, single-day values will be calculated for each day. First, the L_x which define the moving path length of east-west will be calculated by Eq. 4 for that day. The daily path length is regressed against the daily average WS to quantify the effect of increasing WS on the east-west moving path length.

Since the daily movement of the UHICP in latitude is not very significant compared to longitude according to the results of previous studies (Chen et al., 2018). Therefore, in terms of latitude movement, this study average the hourly latitude centroid points ($Loc_{c\_y(hour)}$) to obtain the monthly latitude centroid point ($Loc_{c\_y(month)}$) by Eq. 8. By averaging over a long period of time, the difference of the UHICP in latitude can be recognized, present the vertical movement in latitude under different CCT in different periods (Fig. 8).

$$Loc_{c\_y(month)} = \frac{\sum_{i=1}^{n} Loc_{c\_y(hour)}}{n} \quad \text{(Eq 8)}$$

$Loc_{c\_y(hour)}$:*Hourly latitude location of the UHI centroid points*
$Loc_{c\_y(month)}$:*Average latitude location of the UHI centroid points in periods*

3. Results

3.1. Movement characteristics of UHI centroid points

The UHI is a dynamic phenomenon and will not always occur in the same distribution pattern in the city. In the past studies, it was also found that the UHI has dynamic movement in different areas. For example, a study in Tokyo, Japan, found significant differences in the UHI patterns between summer and winter through standard deviation of Ta. During summer, the monthly average UHI area with high deviation extended from the coastal area inland northwards. Throughout the day, the UHI concentrated along the coast at night, spreading inland after

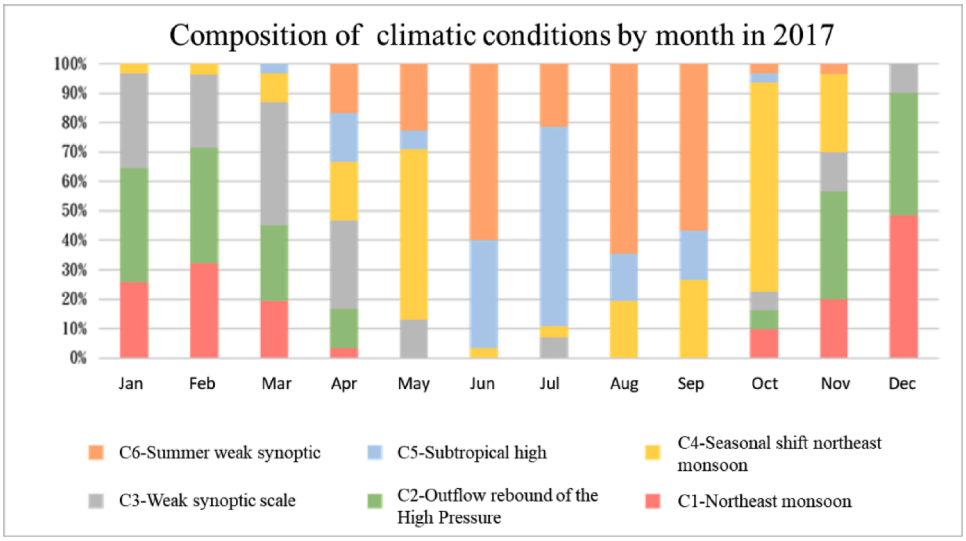

Fig. 7. Composition of climate condition types by Month.

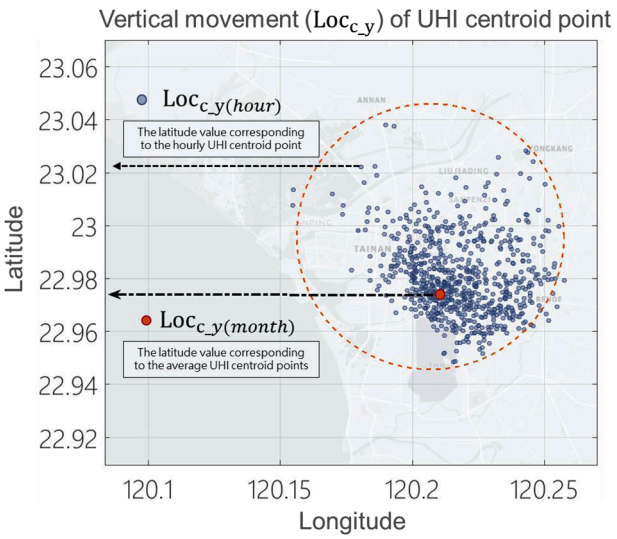

Fig. 8. Schematic calculation of the average latitude of the UHI centroid point.

sunrise, causing the UHI to shift from south to north (Honjo, 2019).

Another study in Beijing also found that the vertical movement of the UHICP is more significant compared to the horizontal, while the normalized difference vegetation index and albedo have a positive effect on the change of UHI movement (Quan et al., 2014). And a past study in Tainan also using HiSAN found that the UHICP shifted was mainly contributed by the different urban environments, including the geographical features, the impervious surface area, the total floor area, and the sky view factor (Chen et al., 2018).

However, past studies have mainly investigated the causes of overall UHI movement. Therefore, in this study, the horizontal and vertical dynamic movements of the UHI will be investigated separately.

3.1.1. Dynamic movement of UHI centroid points in different seasons

This study categorizes the movement of the UHICP into two groups: the hot season (represented by the summer months of June, July, and August) and the cool season (represented by the winter months of December, January, and February). When discussing the hot and cool seasons separately, it becomes evident that the UHICP movement paths on different dates exhibit distinct patterns (Fig. 9).

During the cool season, the s movement tends to be oriented towards the city center in the southern region and forms a more circular path compared to the elongated oval path observed during the hot season. This circular path suggests that the temperature distribution between land and sea variations is less pronounced during the cool season in contrast to the hot season in Tainan.

On the other hand, in the hot season, the overall trend consistently shows an elongated shape predominantly located in the northern region. This elongated shape indicates that the high-temperature area experiences more significant changes between land and sea over time. The northward orientation of the path implies that the high-temperature region is situated more towards the northern side of the study area. In comparison to the hot season, during the cool season, the daily movement paths of the UHICP are more concentrated and tend to be situated southward in the city center area. It is hypothesized that the prevailing strong northeast monsoon during the cool season in the overall environmental context could lead to relatively lower Ta in the northern suburban areas. Consequently, the path of UHICP movement may exhibit a general southward orientation during the cool season.

To further explore this phenomenon, the study employs climate classification and divides climate types into six conditions as mentioned in Section 2.4 to investigate whether the broader environmental wind patterns contribute to the southward deviation of the UHICP movement path.

3.1.2. Wind speed and East-West various distance of UHI centroid point

After conducting daily calculations of the UHICP movement path throughout the year, the L_x were determined by analyzing the maximum and minimum longitude values for each day. It was found that there is not a significant correlation between the L_x of the UHICP and variations in WS, with a correlation coefficient of only 0.042.

To investigate the factors contributing to the L_x of the UHICP on a daily basis, this study employed climate grouping to filter dates and analyzed the average WS of all CWB stations in Tainan. However, the L_x does not demonstrate an increase due to higher WS. The variations in the movement transition of the UHICP from coastal to inland areas during day and night, under the influence of different climate patterns, indicate that the differences in L_x lengths are not solely determined by the magnitude of WS.

3.1.3. Diurnal temperature range and horizontal movement of UHI centroid point

In the previous section, it was observed that WS does not have a significant impact on the L_x of the UHICP during the transition between

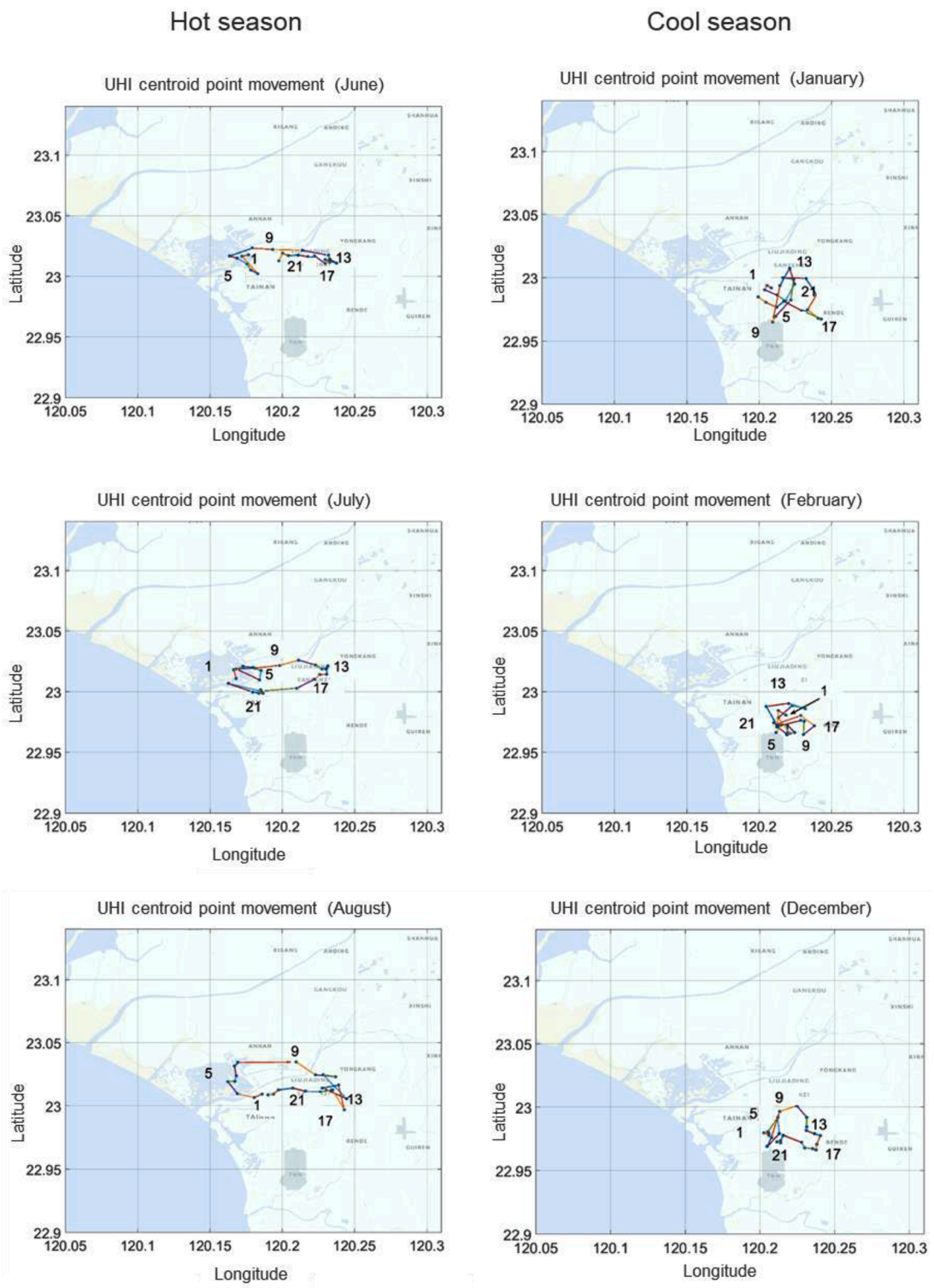

Fig. 9. Hourly UHI centroid point movement paths in hot and cool season.

coastal and inland areas. However, this study noted that the differences in L_x of the UHICP are more pronounced in hot season than cool season.

Therefore, the hypothesis is that the DTR of different days, specifically the difference between the maximum and minimum Ta could be one of the main influencing factors. To analyze this, the DTR and L_x were plotted and examined (Fig. 10).

In the western region of the study area, there is a significant amount of water bodies, and the building density and height are relatively low. On the eastern inland side, there is higher building density and greater use of artificial materials. Due to the higher specific heat capacity of the ocean, the Ta changes caused by the same solar radiation and artificial heat sources result in smaller variations in the overall water temperature.

On the other hand, the specific heat capacity of artificial materials is lower compared to water, making them more susceptible to Ta fluctuations. When the DTR is smaller, the differences between the ocean and land within a day are minimal, causing the UHICP to concentrate in the central area of Tainan. However, when the DTR is larger, the differences

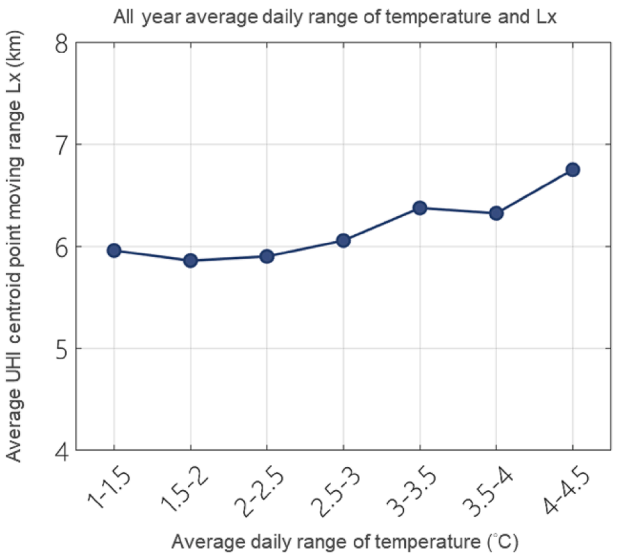

Fig. 10. All year average DTR and UHI centroid point moving range Lx.

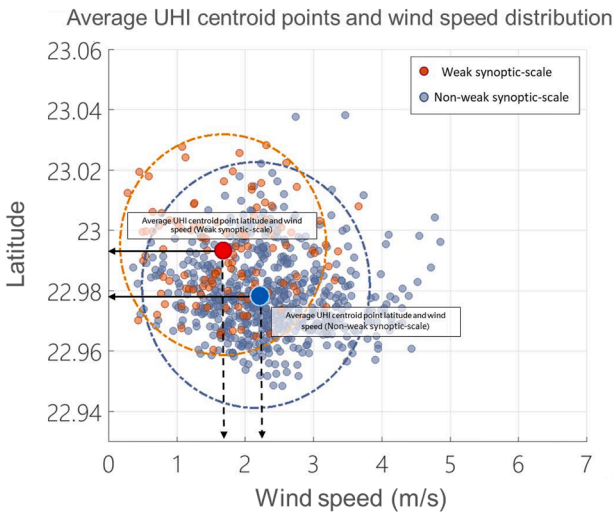

Fig. 11. Monthly distribution of latitude and wind speed of UHI centroid points for different climatic condition types.

between the ocean and land become magnified, leading to greater movement of the UHICP due to varying Ta between ocean and land during day and night.

The study revealed that a larger DTR on a given day corresponds to a greater average L_x of the UHICP, this study also found that in Tainan City, a larger DTR occurs in the hot season than in the cool season. In other words, when the DTR is larger, the UHICP tends to be closer to the western water bodies during nighttime when there is no solar radiation. As solar radiation begins to exert its heating effect during the daytime, the inward movement of the UHICP towards the inland areas becomes more pronounced.

This situation can have an impact on satellite cities located inland outside the city center. When there is a significant Ta difference within a day, the UHICP of Tainan tends to move further inland. This implies that the range of influence caused by high temperatures in Tainan becomes larger and extends deeper into the inland regions.

3.1.4. Wind speed and north-south various distance of high temperature centroid point

This study discovered a phenomenon of north-south displacement in the movement path of the UHICP. By calculating the latitude $Loc_{c\_y(hour)}$ of the UHICP for each hour, this research then established the average latitude $Loc_{c\_y(month)}$ for each month's data. The average latitude coordinates were used to investigate the distribution of the UHICP under various CCT. This approach allows for the characterization of latitude distribution patterns associated with different CCT, simplifying the data for easier discernment.

This study conducted a filter based on CCT, dividing the UHICP data for each month into two categories: weak synoptic scale and non-weak synoptic scale. The weak synoptic scale associated with lower WS (Fig. 11). It is evident that the weak synoptic scale and non-weak synoptic scale exhibit different latitude distribution trends for the UHICP.

Focusing on the changes during the hot season and cool season, the study indicates that the UHICP movement shifts northward during hot season and conversely southward during cool season concentrating around the city center. Analyzing the results based on the $Loc_{c\_y(month)}$, it is evident that, during hot season, the average UHICP of the non-weak synoptic scale is further north compared to the weak synoptic scale. On the contrary, during cool season, the average UHICP of the non-weak synoptic scale tends to be further south than the weak synoptic scale (Fig. 12).

Taking into account the climatic characteristics of the study area, the following explanations can be inferred. During hor season, the

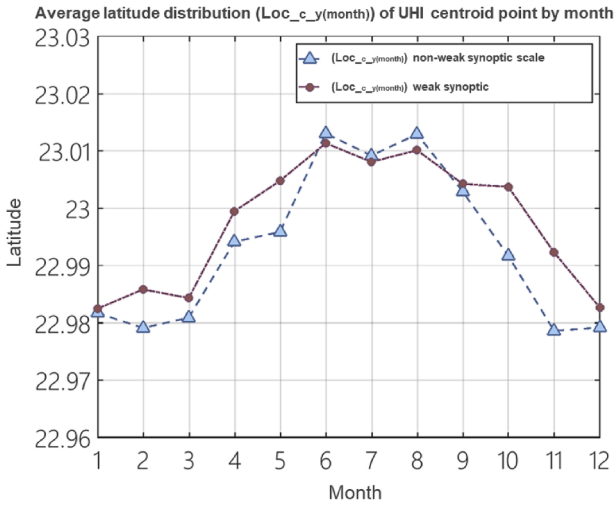

Fig. 12. Distribution of monthly average latitude ($Loc_{c\_y(month)}$) of UHI centroid points for weak synoptic and non-weakly synoptic scale in each month.

prevailing winds in Tainan are southerly winds, and when the weather is non-weak synoptic scale, relatively higher WS result in the average UHICP moving northward. In cool season, the dominant wind directions are northerly; the results also indicate that, compared to the weak synoptic scale, the non-weak synoptic scale tends to have an avera $Loc_{c\_y(month)}$ further south.

Therefore, the study suggests that the distinction between weak synoptic and non-weak synoptic scales lead to variations in WS. Additionally, the study finds that the strength of the prevailing wind direction in different seasons leads to the difference in the vertical distribution of the UHICP.

3.2. Correlation between built environment and thermal conditions

Previous studies have established the effects of built environments on microclimate at different scales, whereas at large scales, land surface temperatures are mostly utilized for analysis (Shahfahad et al., 2022; Xi et al., 2023; Cetin et al., 2024). In this study, due to the use of HiSAN, the effects of built environmental factors on the intensity of UHI can be more accurately described at the urban scale (Chen et al., 2018; Chen et al., 2019). In addition, with the data from the long-term Ta record, the

different effects of daytime and nighttime can be quantified.

In order to investigate the influence of different factors on the thermal conditions in different periods, this section includes correlation analysis based on the percentage of different factors in the buffer area of each measurement point, as well as the UHID. As past studies in Tainan have shown that analyzing the impacts of different factors with Ta data, it can be seen that different urban development factors have different impacts at different buffer area sizes, and among them the 300-meter radius is the one showing the most significant impacts (Chen et al., 2019), therefore, this study follows the 300-meter radius as the setting of the buffer area size for the analysis the correlation between built environment and thermal condition (Table 1).

3.2.1. Proportion of building area

The results of the study indicate that during both daytime and nighttime, areas with a higher proportion of buildings tend to have higher Ta, while areas with a lower proportion of buildings exhibit the opposite trend. The daytime negative correlation reaches 0.24, and the nighttime correlation reaches 0.68 (Fig. 13). According to the calculation of SRL, a higher proportion of building area will result in a larger SRL in a region, leading to an enhanced effect on the WS discounting. In general, a larger percentage of building area is associated with higher UHID and tends to decrease WS.

3.2.2. Proportion of green area

In this study, a significant negative correlation was found between the green area proportion and the UHID, particularly during nighttime, with a correlation coefficient of around -0.64 (Fig. 14). This indicates that the presence of green areas has an effective cooling effect at nighttime, attributed to the evaporative heat dissipation effect of the green areas, helping to reduce heat near the park green areas.

However, during the daytime, the cooling effect resulting from an increased green area appears to be limited, with a correlation coefficient of about -0.1. The study hypothesizes that this limited effect during the daytime may be due to the artificial pavement on the surface of the green areas dilute the effectiveness of heat dissipation from the area.

3.2.3. Proportion of water area

The study reveals findings regarding the impact of water bodies on the urban thermal condition. In the nighttime, a positive correlation is observed between the water body proportion and Ta, with a correlation coefficient of around 0.13 (Fig. 15). This suggests that water bodies are slightly heated at night, as they have a larger specific heat compared to other surfaces and structures. During the night, water bodies release the heat stored during the day, contributing to a warming trend in the urban area.

Conversely, during the daytime, a negative correlation is found between the water body area and Ta, with a correlation coefficient of about -0.52. This indicates that a larger water body area has a cooling effect during the day. The presence of a larger water area enhances overall ground openness, reduces surface roughness, and facilitates good ventilation and diffusion conditions for the wind condition. Moreover, the water body's evaporation contributes to an effective cooling effect during the daytime.

Table 1
Correlation of built environment proportion of area with UHI deviation.

	Building area	Green area	Water area
UHID in Daytime	Low positive relationship (R=0.24)	Low negative relationship (R=-0.1)	Highly negative correlation (R=-0.52)
UHID in Nighttime	Highly positive correlation (R=0.68)	Highly negative correlation (R=-0.64)	Low positive relationship (R=0.13)

3.3. The effect of wind speed on cooling

In this study, by investigating the land cover of Tainan City and the standard WS data of CWB, the SRL of different areas can be obtained, and the predicted WS and the of wind speeds deviation (WSD) at 100 HiSAN measurement points can be obtained on a hourly basis. The correlation between the wind condition and the cooling is analyzed by using the hourly UHID and the WSD at the location of each HiSAN measurement point.

This study highlights the varying impact of WSD on the UHID during different periods. During the daytime, the effect of WSD on reducing the UHID is found to be less effective, with a correlation coefficient of about -0.17. This suggests that solar radiant heat remains the dominant factor influencing Ta during the daytime. The study implies that, in daytime conditions, the effect of ventilation on heat dissipation in the area is not as pronounced.

In contrast, during nighttime, when the influence of solar radiant heat is lower, there is a significant negative correlation between WSD and UHID, with a correlation coefficient of about -0.58. This indicates that good ventilation becomes more effective in decreasing Ta in the area during the nighttime. The cooling effect of WS plays a more significant role due to the increase in WS leads to better evapotranspiration, and better evapotranspiration means that heat and energy are removed more quickly. (Fig. 16).

4. Discussion

4.1. The impact of urban environment on ventilation and thermal condition

The study's findings suggest that addressing the UHI requires a nuanced approach based on the specific environmental factors influencing the thermal condition. While reducing building area might be a direct method to mitigate warming during the daytime, it is acknowledged that constraints related to population growth and urban development make this approach challenging.

This study found the more building areas contribute to warming, both day and night. While compared to areas with less green areas, areas with more green areas have a stronger cooling effect regardless of the daytime, but this effect is more significant at nighttime. This study suggests that the reason for this is that vegetation continues to evaporate during the night, and therefore absorbs more heat energy from the environment than buildings and water bodies. In addition, the surface of some green areas is paved with artificial surfaces such as cement, brick and stone, which will reduce the cooling effect of the green areas during the daytime due to the heating by solar radiation. On the other hand, water has a significant cooling effect during the day and warming effect at night. The reason is the high specific heat property of water, during the daytime, water can absorb a large amount of heat due to solar radiation, and at night, this heat is slowly released into the environment.

As for the ventilation effect of environmental factors on the predicted WS, in the investigation of the correlation between thermal and wind conditions, it is found that the wind speed has a negative correlation with the temperature in both daytime and nighttime, but the correlation is more obvious in the nighttime. Therefore, when planning urban ventilation and cooling strategies, the distribution of open spaces within the construction site will need to be further optimized for the ventilation and dispersion conditions of the area.

4.2. Relationship between climate condition types and thermal condition characteristics

In the past, research on the temporal and spatial variations of Ta in the Tainan through HiSAN primarily focused on investigating regional patterns (Chen et al., 2018; Chen et al., 2019). The study highlights the novel contribution of classifying dates using CCT to understand the

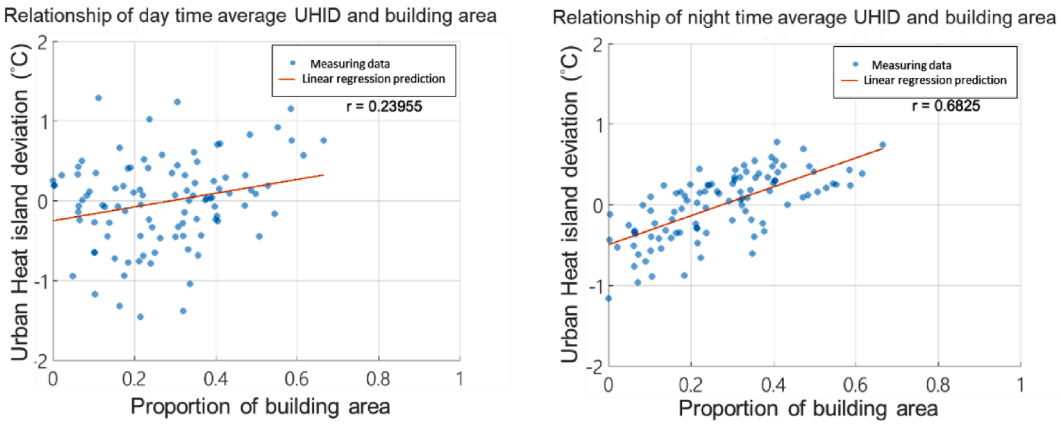

Fig. 13. Relationship between proportion of building area and UHID.

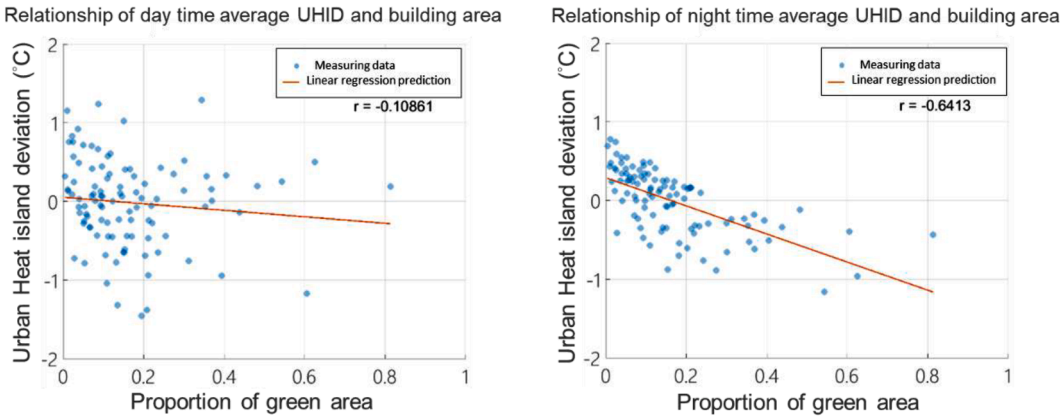

Fig 14. Relationship between proportion of green area and UHID.

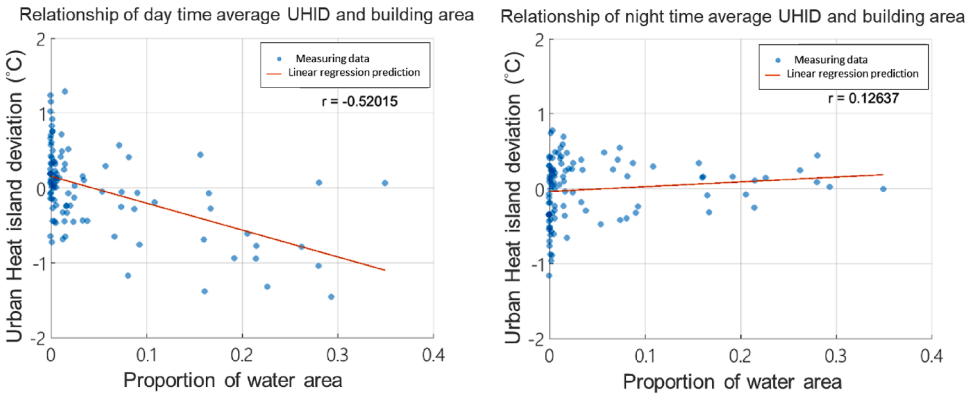

Fig 15. Relationship between proportion of water area and UHID.

temporal and spatial variations of Ta in Tainan and revealing that different heat distribution patterns can emerge within the same month based on whether the dates fall under a weak synoptic scale climatic type. This finding underscores the importance of considering climatic conditions for a more comprehensive understanding of urban thermal conditions.

The study also discovers the impact of CCT on the background wind condition over a large scale. While the research focused on specific CCT, there is a suggestion for future studies to define climatic information more meticulously and incorporate additional climatic factors for classification analysis. This approach could provide a more nuanced understanding of the interaction between CCT and urban thermal conditions, ultimately aiding in the identification of optimal mitigation strategies for UHI in different scenario.

4.3. Application in urban planning and sustainable development

For the application in urban planning, areas used mainly during the daytime, such as industries, commercial areas and schools, they are recommended to be located closer to the sea for a more comfortable thermal condition, and a land cover plan with water bodies as the main focus, supplemented by green areas, should be set up within a radius of 300-meters of the built-up areas. For residential areas that are mainly occupied at nighttime, it is recommended to be located inland areas that

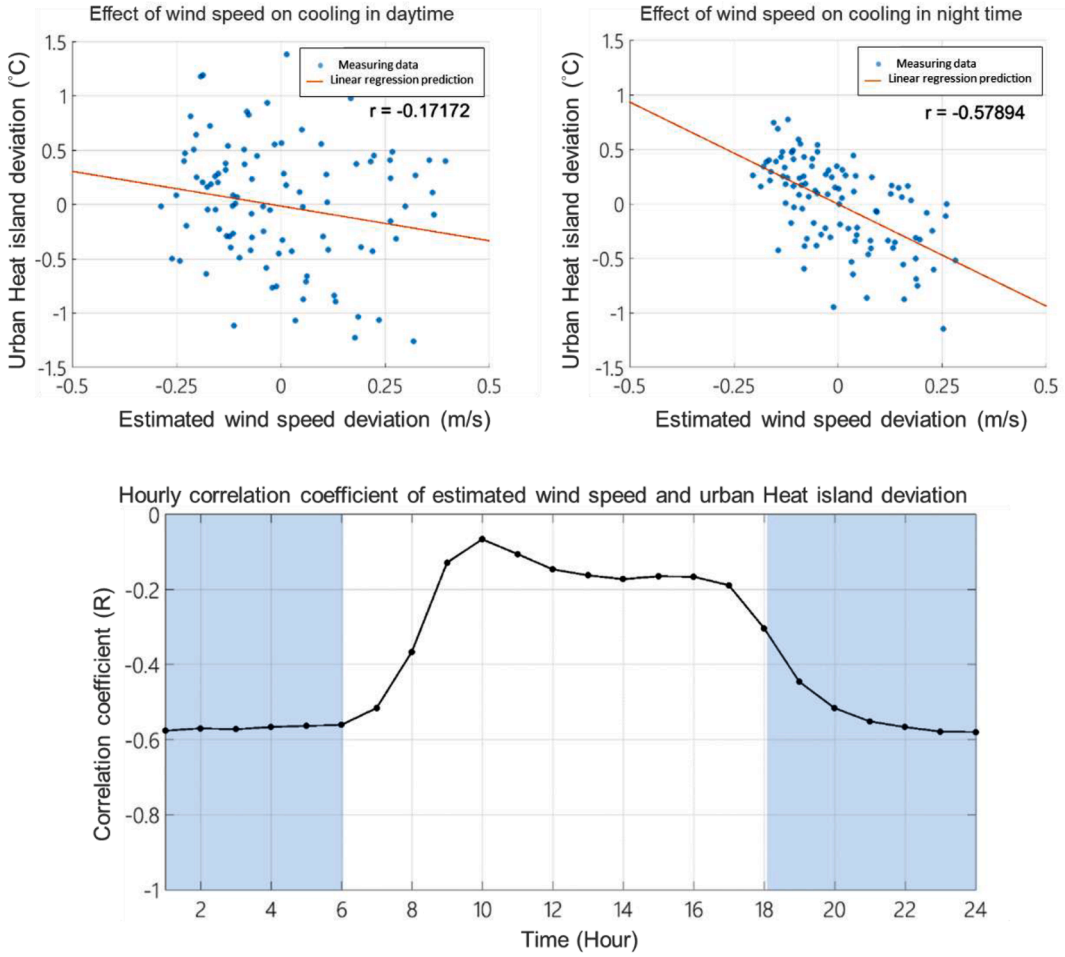

Fig 16. Relationship between estimated wind speed deviation area and UHID.

have lower Ta at nighttime and better cooling effect by ventilation, and to increase green areas within a radius of 300-meters in order to maintain the range and effect of green areas in cooling.

Past studies using HiSAN have also suggested that scattered green areas of the same area can have a better regional cooling effect by increasing the edge length of contact with the surrounding area, while buildings with the same floor area should be more concentrated to minimize the chance of contact with the surrounding environment (Chen et al., 2019).

In addition, this study found that past regulations focused on building configuration. Regulating building location, façade area, and gap distance can improve ventilation and reduce temperatures. However, ventilation alone isn't the sole solution for urban temperature reduction; surface morphology also plays a crucial role. Green areas, water bodies and open areas can be strategically planned to cool urban areas and propose UHI mitigation strategies early in urban planning stages.

In addition, the findings of this study can also be applied to the long-term sustainable development goals of Tainan City. In terms of economic upgrading, the implementation of cooling strategies in hot spots can reduce the energy cost of air-conditioning (Hwang et al., 2017) as well as the cost of agricultural production (Hung et al., 2023). In terms of transportation upgrading, the increased green areas can provide more comfortable walking space on the roads (De Quadros and Mizgier, 2023), and also reduce the possibility of car accidents (Park et al., 2021). In terms of health upgrades, the benefits of increased green areas are not only cooling, but also improving the air quality of the city, while the benefits of ventilation improvements are better air dispersion, which further reduces the spreading of disease (Ng, 2009).

In terms of environmental sustainable development, the recommendations of this study on land cover and ventilation can reduce energy consumption, air pollution concentration, and discomfort by avoiding the formation of high temperatures and reducing SRL.

In terms of warmth sustainable, through the distribution of UHI at different times produced by this study, the government will be able to recognize the situation of high temperature exposure more effectively and react more quickly to take care of highly vulnerable groups such as the elderly and children. Finally, in the aspect of education sustainable, the recommendations of this study can be used to create a green campus with better comfortable condition, and the results of the study can raise the awareness of teachers and students on the threats of UHI, and to promote the application of heat-reduction solutions.

4.4. Future research potential and limitation

4.4.1. Reseaech limitation

The limitation of this study is on the WS prediction and verification, this study uses the SRL and exponential wind profile to predict the WS by gridding, however, the above prediction WS is only verified by short-term measurement, the accuracy of the subsequent study still needs to be validated by a more long-term measurement.

In addition, in the analysis of the state of the environmental buffer area, this study focuses on the analysis of the Ta and WS caused by the two-dimensional planar proportion, no further analysis of the factors at heights. Relevant characteristics such as height to width ratio and sky view factor of the buildings can be analyzed in the following study.

Finally, in the improvement of HiSAN, the major challenge of this measurement network is in the collection of data and the power supply of the instrument. The battery time limit is about two months, which costs a lot of time and human resource, and subsequently the research can use low power consumption instruments with IOT technology for measurement, so as to facilitate the use of real-time data.

4.4.2. Future research potential

The HiSAN has been used to observe thermal condition characteristics in urban areas (Chen et al., 2018; Chen et al., 2019; Lau et al., 2023), and has been widely utilized in exploratory studies that include air-conditioning energy consumption (Hwang et al., 2020) and evaluation of solar power generation potential (Chao et al., 2021), as well as air quality assessment (Yu et al., 2020) and machine learning to analyze thermal conditions (Lau & Lin, 2024).

The HiSAN can be well utilized to observe different factors for microclimate comprehension because of the characteristics of a high number of measurement points, high density, and distribution in diverse built-up environments. Therefore, the research topics for the future development potential of HiSAN could include the following:

First, combining different simulation models, such as weather research and forecasting (WRF) and large-eddy simulation (LES), and using them to assess the risk of extreme climate in urban areas, as well as the interactions between wind and thermal conditions, this issue will effectively improve the accuracy of large-scale Ta predictions and facilitate the calibration of the model results at a large number of measurement points.

Second, HiSAN can also be used as an important information for exploring the public health status of urban environments, such as exploring the relationship between the distribution of air pollution and Ta, the intensity of high temperature exposure and the impact on the health of residents, etc., which allows the information with a large database of temperature to be analyzed in combination with the factors from the natural sciences and social sciences, which is a very important issue in the development of sustainable cities.

Third, with regard to urban morphological description tools other than area size, such as local climate zone (LCZ) and landscape ecological metrics (LEM), HiSAN will also have sufficient microclimate information to analyze the relationship between urban planning patterns and environmental comfort (Chen et al., 2024), so as to propose policy recommendations to promote urban cooling, and put forward practicable UHI mitigation strategies for cities.

5. Conclusion

This study delves into the intricate relationship between urban environmental factors, CCT, and their combined impact on thermal and wind conditions in Tainan City. Several key findings emerge through an extensive analysis of various parameters and correlations.

First, the study reveals the imapct of CCT and thermal conditions on UHI movement characteristics. It determines the relationship between WS and the north-south movement of the UHICP, as well as the effect of the DTR and the east-west movement distance.

The strength of prevailing winds influences the location of the UHICP, shifting more northward during hot season and more southward during in cool season on non-weak synoptic scales with stronger WS. The UHICP movement paths are circular near the city center in the hot season, the Lx are elongated due to significant DTR. In the cool season the Lx will be shorter due to less DTR.

Concerning the impact of different built environment factors on the thermal condition, the study finds that the proportion of building area is positively correlated with both daytime and nighttime temperatures. Higher building area leads to higher UHID throughout the day, with more pronounced warming at night due to buildings have more heat storage than the surrounding environment. The proportion of green area showed a negative correlation with UHID both during the day and at night, but had a more pronounced cooling effect at night than during the day, because of the continuous evapotranspiration of vegetations at nighttime, which can absorb more heat energy from the surrounding environment than buildings and water bodies. Trends for water bodies differ between daytime and nighttime, water bodies have a warming effect on surroundings due to their high specific heat in nighttime, while during the daytime, the water bodies have a cooling effect on the city through good ventilation and improved evaporative cooling.

As for the correlation between wind and thermal conditions, a negative correlation was found between WSD and UHID both during the daytime and nighttime, but the correlation was more significant during the nighttime. This indicates that stronger WS will have a better cooling effect during the nighttime.

In conclusion, this study provides insights into the intricate dynamics between urban built environmental factors, CCT, and their collective impact on thermal and wind conditions. The findings underscore the significance of urban planning strategies considering building, green areas, water bodies, and wind patterns to effectively mitigate UHI. As cities grow and face increasing heat challenges, these findings can inform sustainable urban development and climate adaptation strategies for creating more livable and comfortable urban environments.

CRediT authorship contribution statement

Yu-Cheng Chen: Writing – original draft, Methodology, Conceptualization. **Kai-Shan Hou:** Writing – review & editing, Validation, Methodology. **Yu-Jie Liao:** Resources, Investigation. **Tsuyoshi Honjo:** Visualization, Supervision. **Fang-Yi Cheng:** Software, Formal analysis. **Tzu-Ping Lin:** Writing – review & editing, Supervision.

Declaration of competing interest

The authors declare no conflict of interest, and they have no known competing financial interests or personal relationships that could have appeared to influence the work reported in this paper.

Data availability

Data will be made available on request.

Acknowledgments

The authors would like to thank the National Science and Technology Council of Taiwan for financially supporting this research under Contract No. 111-2221-E-006-053-MY3, No. 112-2119-M-865-004- and No. 111-2221-E-343-001-MY3. Thanks to the additional support of The Taiwan Climate Change Projection Information and Adaptation Knowledge Platform (TCCIP).

References

Al-Obaidi, I., Rayburg, S., Półrolniczak, M., & Neave, M. (2021). Assessing the impact of wind conditions on urban heat islands in large Australian Cities. *Journal of Ecological Engineering, 22*(11), 1–15.

An, N., Dou, J., González-Cruz, J. E., Bornstein, R. D., Miao, S., & Li, L. (2020). An observational case study of synergies between an intense heat wave and the urban heat island in Beijing. *Journal of Applied Meteorology and Climatology, 59*, 605–620.

Anjos, M., Targino, A. C., Krecl, P., Oukawa, G. Y., & Braga, R. F. (2020). Analysis of the urban heat island under different synoptic patterns using local climate zones. *Building and Environment, 185*, Article 107268.

Bagiorgas, H. S., Mihalakakou, G., & Matthopoulos, D. (2008). A statistical analysis of wind speed distributions in the area of Western Greece. *International Journal of Green Energy, 5*(1), 120–137.

Baker, L. A., Brazel, A. J., Selover, N., Martin, C., McIntyre, N., Steiner, F. R., & Musacchio, L. (2002). Urbanization and warming of phoenix (Arizona, USA): Impacts, feedbacks and mitigation. *Urban Ecosystems, 6*(3), 183–203.

Cecilia, A., Casasanta, G., Petenko, I., Conidi, A., & Argentini, S. (2023). Measuring the urban heat island of Rome through a dense weather station network and remote sensing imperviousness data. *Urban Climate, 47*, Article 101355.

Central Weather Bureau of Taiwan. (2021). Monthly report on climate system. Available at: https://e-service.cwb.gov.tw/HistoryDataQuery/index.jsp.
Cetin, M., Ozenen Kavlak, M., Senyel Kurkcuoglu, M. A., Ozturkm, G. B., Cabuk, S. N., & Cabuk, A. (2024). Determination of land surface temperature and urban heat island effects with remote sensing capabilities: The case of Kayseri. *Türkiye. Natural Hazards*. https://doi.org/10.1007/s11069-024-06431-5
Chao, C. C., Hung, K. A., Chen, S. Y., Lin, F. Y., & Lin, T. P. (2021). Application of a high-density temperature measurement system for the management of the Kaohsiung house project. *Sustainability, 13*(2), 960.
Chen, Y. C., Chen, C. Y., Matzarakis, A., Liu, K. J., & Lin, T. P. (2016). Modeling of mean radiant temperature based on comparison of airborne remote sensing data with surface measured data. *Atmospheric Research, 174*, 151–159.
Chen, Y. C., Fröhlich, D., Matzarakis, A., & Lin, T. P. (2017). Urban roughness estimation based on digital building models for urban wind and thermal condition estimation—Application of the SkyHelios model. *Atmosphere, 8*(12), 247.
Chen, Y. C., Liao, Y. J., Yao, C. K., Honjo, T., Wang, C. K., & Lin, T. P. (2019). The application of a high-density street-level air temperature observation network (HiSAN): The relationship between air temperature, urban development, and geographic features. *Science of The Total Environment, 685*, 710–722.
Chen, Y. C., Lo, T. W., Shih, W. Y., Lin, T. P., & Hung, K. A. (2024). Assessment of urban thermal environment using the combination of Local Climate Zone (LCZ) and Landscape Ecological Metrics (LEM) in Taipei City. *Journal of Urban Planning and Development, 150*(2), Article 05024004.
Chen, Y. C., Yao, C. K., Honjo, T., & Lin, T. P. (2018). The application of a high-density street-level air temperature observation network (HiSAN): Dynamic variation characteristics ofurban heat island in Tainan, Taiwan. *Science of The Total Environment, 626*, 555–566.
Cheng, F. Y., & Hsu, C. H. (2019). Long-term variations in PM2.5 concentrations under changing meteorological conditions in Taiwan. *Scientific Reports, 9*, 6635.
Counihan, J. (1975). Adiabatic atmospheric boundary layers: A review and analysis of data from the period 1880-1972. *Atmospheric Environment, 9*(10), 871–905.
de Quadros, B. M., & Mizgier, M. G. O. (2023). Urban green infrastructures to improve pedestrian thermal comfort: A systematic review. *Urban Forestry & Urban Greening, 88*, Article 128091.
Heusinkveld, B. G., Hove, L. W. A. V., Jacobs, C. M. J., Steeneveld, G. J., Elbers, J. A., Moors, E. J., & Holtslag, A. A. M (2010). Use of a mobile platform for assessing urban heat stress in Rotterdam. In *Proc. 7th Conf. on Biometeorology, Freiburg, Germany* (pp. 433–438).
Hintz, K. S., Vedel, H., Kaas, E., & Nielsen, N. W. (2020). Estimation of wind speed and roughness length using smartphones: Method and quality assessment. *Journal of Atmospheric and Oceanic Technology, 37*, 1319–1332.
Honjo, T. (2019). Analysis of urban heat island movement and intensity in Tokyo metropolitan area by AMeDAS data. *Journal of Agricultural Meteorology, 75*(2), 84–91.
Hung, K. A., Hsu, Y. W., Chen, Y. C., & Lin, T. P. (2023). Influence of microclimate control on the growth of asparagus under greenhouse in tropical climates. *International Journal of Biometeorology, 67*(7), 1225–1235.
Hwang, R. L., Lin, C. Y., & Huang, K. T. (2017). Spatial and temporal analysis of urban heat island and global warming on residential thermal comfort and cooling energy in Taiwan. *Energy and Buildings, 152*, 804–812.
Hwang, R. L., Lin, T. P., & Lin, F. Y. (2020). Evaluation and mapping of building overheating risk and air conditioning use due to the urban heat island effect. *Journal of Building Engineering, 32*, Article 101726.
Japan Sustainable Building Consortium. (2014). CASBEE Technical Manual 2014 Edition; CASBEE for building (New Construction). *Institute for Built Environment and Carbon Neutral for SDGs*. Available at: https://www.ibec.or.jp/CASBEE/english/download/CASBEE-BD(NC)e_2014manual.pdf.
Kaloustian, N., & Bechtel, B. (2016). Local climatic zoning and urban heat island in Beirut. *Procedia Engineering, 169*, 216–223.
Kondo, J., & Yamazawa, H. (1986). Aerodynamic roughness over an inhomogeneous ground surface. *Boundary-Layer Meteorology, 35*, 331–348.
Kwok, Y. T., de Munck, C., Lau, K. K., & Ng, E. (2022). To what extent can urban ventilation features cool a compact built-up environment during a prolonged heatwave? A mesoscale numerical modelling study for Hong Kong. *Sustainable Cities and Society, 77*, Article 103541.
Lau, T. K., & Lin, T. P. (2024). Investigating the relationship between air temperature and the intensity of urban development using on-site measurement, satellite imagery and machine learning. *Sustainable Cities and Society, 100*, Article 104982.
Lau, T. K., Chen, Y. C., & Lin, T. P. (2023). Application of local climate zones combined with machine learning to predict the impact of urban structure patterns on thermal environmen. *Urban Climate, 52*, Article 101731.
Lin, T. P., Chen, Y. C., & Matzarakis, A. (2017). Urban thermal stress climatic mapping: Combination of long-term climate data and thermal stress risk evaluation. *Sustainable Cities and Society, 34*, 12–21.
Liu, L., Lin, Y., Liu, J., Wang, L., Wang, D., Shui, T., Chen, X., & Wu, Q. (2017). Analysis of local-scale urban heat island characteristics using an integrated method of mobile measurement and GIS-based spatial interpolation. *Building and Environment, 117*, 191–207.
Luo, F., Yang, Y., Zong, L., & Bi, X. (2023). The interactions between urban heat island and heat waves amplify urban warming in Guangzhou, China: Roles of urban ventilation and local climate zones. *Frontiers in Environmental Science, 11*, Article 1084473.
Mikami, T., Yamato, H., & Extended-METROS Research Group. (2011). High-resolution temperature observations using extended-METROS in the Tokyo metropolitan area and their urban climatological significance. *Journal of Geography, 120*(2), 317–324.
Müller, N., Kuttler, W., & Barlag, A. B. (2014). Counteracting urban climate change: adaptation measures and their effect on thermal comfort. *Theoretical and Applied Climatology, 115*, 243–257.
Murakami, S., Matsunawa, K., Mochida, A., Morikawa, Y., Hayashi, H., & Oguro, M. (2007). Development of wind environment data-base for comprehensive assessment system for building environmental efficiency on heat island relaxation. *AIJ journal of technology and design, 13*(26), 659–662.
Ng, E. (2004). Regulate for light, air and healthy living – Part II regulating the provision of natural light and ventilation of buildings in Hong Kong. *Hong Kong Institute of Architects Journal, 37*, 14–27.
Ng, E. (2009). Policies and technical guidelines for urban planning of high-density cities-air ventilation assessment (AVA) of Hong Kong. *Building and Environment, 44*(7), 1478–1488.
Oke, T. R. (1982). The energetic basis of the urban heat island. *Quarterly Journal of the Royal Meteorological Society, 108*, 1–24.
Oke, T. R., Mills, G., Christen, A., & Voogt, J. A. (2017). *Urban Climates*. U.K: Cambridge University Press.
Oyedepo, O., Adaramola, S., & Paul, S. (2012). Analysis of wind speed data and wind energy potential in three selected locations in south-east Nigeria. *International Journal of Energy and Environmental Engineering, 3*(7), 1–11.
Park, J., Choi, Y., & Chae, Y. (2021). Heatwave impacts on traffic accidents by time-of-day and age of casualties in five urban areas in South Korea. *Urban Climate, 39*, Article 100917.
Quan, J., Chen, Y., Zhan, W., Wang, J., Voogt, J., & Wang, M. (2014). Multi-temporal trajectory of the urban heat island centroid in Beijing, China based on a Gaussian volume model. *Remote Sensing of Environment, 149*, 33–46.
Rajagopalan, P., Lim, K. C., & Jamei, E. (2014). Urban heat island and wind flow characteristics of a tropical city. *Solar Energy, 107*, 159–170.
Rasham, A. M. (2016). Analysis of wind speed data and annual energy potential at three locations in Iraq. *International Journal of Computers and Application, 137*(11), 0975–8887.
Richard, Y., Pohl, B., Rega, M., Pergaud, J., Thévenin, T., Emery, J., Dudek, J., Vairet, T., Zito, S., & Chateau-Smith, C. (2021). Is Urban Heat Island intensity higher during hot spells and heat waves (Dijon, France, 2014-2019)? *Urban Climate, 35*, Article 100747.
Saaroni, H., Ben-Dor, E., Bitan, A., & Potchter, O. (2000). Spatial distribution and microscale characteristics of the urban heat island in Tel-Aviv, Israel. *Landscape and Urban Planning, 48*, 1–8.
Sangiorgio, V., Fiorito, F., & Santamouris, M. (2020). Development of a holistic urban heat island evaluation methodology. *Scientific Reports, 10*, 17913.
Shahfahad, N., Towfiqul Islam, M. W., Mallick, A. R. M., J., & Rahman, A. (2022). Land use/land cover change and its impact on surface urban heat island and urban thermal comfort in a metropolitan city. *Urban Climate, 41*, Article 101052.
Shen, C., Shen, A., Cui, Y., Chen, X., Liu, Y., Fan, Q., Chan, P., Tian, C., Wang, C., Lan, J., Gao, M., Li, X., & Wu, J. (2022). Spatializing the roughness length of heterogeneous urban underlying surfaces to improve the WRF simulation-part 1: A review of morphological methods and model evaluation. *Atmospheric Environment, 270*, Article 118874.
Shi, Z., Yang, J., Zhang, Y., Xiao, X., & Xia, J. C. (2022). Urban ventilation corridors and spatiotemporal divergence patterns of urban heat island intensity: A local climate zone perspective. *Environmental Science and Pollution Research, 29*(49), 74394–74406.
Sobstyl, J. M., Emig, T., Qomi, M. J. A., Ulm, F. J., & Pellenq, R. J. (2018). Role of city texture in Urban Heat Islands at nighttime. *Physical Review Letters, 120*(10), Article 108701.
Son, N. T., Chen, C. F., Chen, C. R., Thanh, B. X., & Vuong, T. H. (2017). Assessment of urbanization and urban heat islands in Ho Chi MinhCity, Vietnam using Landsat data. *Sustainable Cities and Society, 30*, 150–161.
Weerasuriya, A. U., Tse, K. T., Zhang, X., & Kwok, K. C. S. (2008). Integrating twisted wind profiles to Air Ventilation Assessment (AVA): The current status. *Building and Environment, 135*(1), 297–307.
Wong, M. S., Nichol, J. E., To, P. H., & Wang, J. (2010). A simple method for designation of urban ventilation corridors and its application to urban heat island analysis. *Building and Environment, 45*(8), 1880–1889.
Xi, Z., Li, C., Zhou, L., Yang, H., & Burghardt, R. (2023). Built environment influences on urban climate resilience: Evidence from extreme heat events in Macau. *Science of The Total Environment, 859*, Article 160270.
Yu, S. Y., Matzarakis, A., & Lin, T. P. (2020). A study of the thermal environment and air quality in hot–humid regions during running events in Southern Taiwan. *Atmosphere, 11*(10), 1101.
Yuan, C., & Ng, E. (2012). Building porosity for better urban ventilation in high-density cities - A computational parametric study. *Building and Environment, 50*, 176–189.
Zong, L., Liu, S., Yang, Y., Ren, G., Yu, M., Zhang, Y., & Li, Y. (2021). Synergistic influence of local climate zones and wind speeds on the urban heat island and heat waves in the megacity of beijing, China. *Frontiers in Earth Science, 9*, 458.